NASA TECHNICAL NOTE

NASA TN D-4418

C.1

NASA TN D-4418

COLD-AIR INVESTIGATION OF A TURBINE FOR HIGH-TEMPERATURE ENGINE APPLICATION

II. Detailed Analytical and Experimental Investigation of Stator Performance

by Herman W. Prust, Jr., Harold J. Schum, and Frank P. Behning

Lewis Research Center
Cleveland, Ohio

NATIONAL AERONAUTICS AND SPACE ADMINISTRATION • WASHINGTON, D. C. • FEBRUARY 1968

COLD-AIR INVESTIGATION OF A TURBINE FOR HIGH-TEMPERATURE ENGINE APPLICATION

II. DETAILED ANALYTICAL AND EXPERIMENTAL INVESTIGATION OF STATOR PERFORMANCE

By Herman W. Prust, Jr., Harold J. Schum, and Frank P. Behning

Lewis Research Center
Cleveland, Ohio

NATIONAL AERONAUTICS AND SPACE ADMINISTRATION

For sale by the Clearinghouse for Federal Scientific and Technical Information
Springfield, Virginia 22151 – CFSTI price $3.00

COLD-AIR INVESTIGATION OF A TURBINE FOR HIGH-TEMPERATURE ENGINE APPLICATION

II. DETAILED ANALYTICAL AND EXPERIMENTAL INVESTIGATION OF STATOR PERFORMANCE

by Herman W. Prust, Jr., Harold J. Schum, and Frank P. Behning

Lewis Research Center

SUMMARY

A detailed investigation was made to determine the effects on turbine stator performance of the blade features of low solidity and large profile and trailing-edge thicknesses. These features are desired for blading suitable for cooled turbine application.

Boundary-layer loss parameters and related loss coefficients were obtained for a stator with these blade features. Experimental loss coefficients for two other stators with thinner blade profiles and higher solidities than the subject blading were also obtained from referenced experimental data. In addition, analytical values of loss coefficients for the subject and one of the reference stators were computed.

At design mean-section critical velocity ratio of 0.790, the experimental results for the subject stator based on annular-sector data show an annular-sector, after-mix, kinetic-energy loss coefficient of approximately 0.05 (equivalent to an efficiency of 0.95). The experimental performance of this stator was compared with the estimated performance of two stators comparable in other respects but with thinner profiles and higher solidities than the subject blading. This comparison indicated that the performance of the subject blading was not significantly affected by increased profile thickness, and that the mean-radius solidity of the subject blading of 1.39 was not too low for good performance.

Good agreement was obtained between experimental and analytical mean-section performance for the subject stator and one of the reference stator bladings. These analytical results indicate that the large trailing-edge blockage of the subject stator (about 10 percent) caused a significant loss, amounting to about 1 percent of the kinetic energy available to the stator.

Rather poor agreement was obtained for the subject stator between experimental annular-sector loss obtained from annular-sector data and annular-sector loss predicted from mean-section data. The after-mix kinetic energy loss coefficient obtained from radial integration was 0.010 (about 23 percent) larger than the predicted value at design critical velocity ratio.

INTRODUCTION

The need for improved gas turbine engine performance has been reemphasized by the advent of new types of aircraft such as the supersonic transport. Studies such as reference 1 show that significant improvements in engine performance can be obtained with increased turbine-inlet temperatures. Generally, turbine-inlet temperatures are limited by the allowable blade stress levels of the best available materials. Increased inlet temperatures can be obtained, however, if some effective means of blade cooling can be employed. The cooling scheme most commonly considered bleeds relatively cool air from the compressor, directs it through the turbine blading for cooling purposes, and then discharges it back into the main gas stream.

When this cooling method is employed, it is necessary (or desirable) to use blade shapes and solidities which are compromised from those considered optimum for best aerodynamic performance. Blade profile thicknesses should be greater than optimum to provide adequate space inside the blading for coolant flow passages. Blunt leading and trailing edges are required so that adequate cooling flow may be applied to these critical areas. In addition, lower than optimum blade solidity is desired to reduce the number of blades so that the required coolant flow may be reduced.

Maximum gain can be realized from this cooling method, if the cycle losses sustained in supplying the coolant flow to the blading and the aerodynamic losses resulting from compromising blade shapes and introducing coolant flow into the main gas stream are minimized. Although considerable research was done by NACA and others in the general area of turbine cooling, the nature and magnitude of the aerodynamic losses associated with cooled blading have not been well defined. Thus, the need for additional research to better understand these losses was indicated. Accordingly, as discussed in reference 2, the turbine research program at Lewis Research Center was expanded to include the study of the problem of aerodynamic losses and other problem areas associated with turbines for high-temperature application.

In reference 2, the turbine design and an experimental investigation to determine the overall performance characteristics, such as weight flow and the outlet flow angles of the stator component of a turbine with physical features suited for high-temperature application, are reported. In addition, blade-surface static pressure distributions were obtained. The results showed that the stator passed design equivalent flow at design pressure ratio, that the measured outlet flow angle agreed closely with the design outlet flow angle for a range of pressure ratios, and that the experimentally obtained blade-surface velocities agreed fairly well with the blade-surface velocities predicted by the design procedure.

The subject investigation is an extension of the investigation of reference 2, in that detailed experimental and analytical boundary-layer loss characteristics and related loss

coefficients for the stator were determined. In addition, the specific effects on stator performance of increased profile and trailing-edge thicknesses, and reduced solidity, relative to more conventional blading, were examined.

Circumferential total-pressure surveys at a sufficient number of radii to adequately cover an annular sector were made immediately downstream of the blade trailing edge to obtain data for computing the experimental boundary-layer loss characteristics for the subject stator. Surveys were made using ambient inlet air at four different stator pressure ratios, corresponding to downstream critical velocity ratios at the hub section of 0.5, 0.7, 0.896 (design), and 1.1.

Boundary-layer loss parameters and related loss coefficients are reported for the subject stator. Also, experimentally determined values of loss coefficients for two reference stators with thinner blade profiles and different solidities than the subject blading are reported and compared with similar values for the subject stator. In addition, analytical values of loss coefficients for the subject stator and one of the reference stators are reported and compared with experimental values of loss coefficients.

The calculation methods and procedures of references 3 to 6 were used as guides for obtaining the experimental and analytical results. For the convenience of the reader, these calculation methods and procedures are summarized in appendixes B and C. (Symbols are defined in appendix A.)

APPARATUS AND INSTRUMENTATION

This facility is essentially the same as that described in detail in reference 2, except that the forward side of the plenum was opened to the atmosphere. The laboratory exhaust system provided the suction required to establish flow through the stator blading. A cross-sectional schematic of the test facility used in this investigation is shown in figure 1.

The full annular stator blade cascade, compromising 50 blades, is shown in figure 2 with the downstream ducting removed. In figure 3 the mean-section blade profile of the subject blading is shown together with the mean-section profiles of the bladings of references 4 and 5, which were designed without considerations for cooling. As shown by figure 3, the subject stator blades were somewhat unconventional. The profiles, including trailing-edge thicknesses, were thicker than customary, as dictated by blade-cooling considerations. The subject stator blades were of free-vortex design, with curved-back suction surfaces downstream of the throat. Design after-mix turning angle was 67° from axial at the mean radius. A complete description of the stator blade design is given in reference 2. Pertinent dimensions are as follows:

Tip diameter, in. (cm)	30.00 (76.2)
Hub-tip radius ratio,	0.733
Mean-radius pitch, s_m, in. (cm)	1.63 (4.14)
Mean-radius chord, c_m, in. (cm)	2.26 (5.74)
Leading-edge radius, in. (cm)	0.150 (0.381)
Trailing-edge radius, in. (cm)	0.035 (0.089)
Maximum thickness, in. (cm)	0.500 (1.27)
Solidity, c_m/s_m	1.39

Total-pressure, static-pressure, and temperature measurements were made in the axial-circumferential locations shown in figure 1. The inlet measuring station (station 0) was located one blade chord upstream of the stator blades. Air-inlet temperature was measured by the use of two rakes, each with five copper-constantan thermocouples,

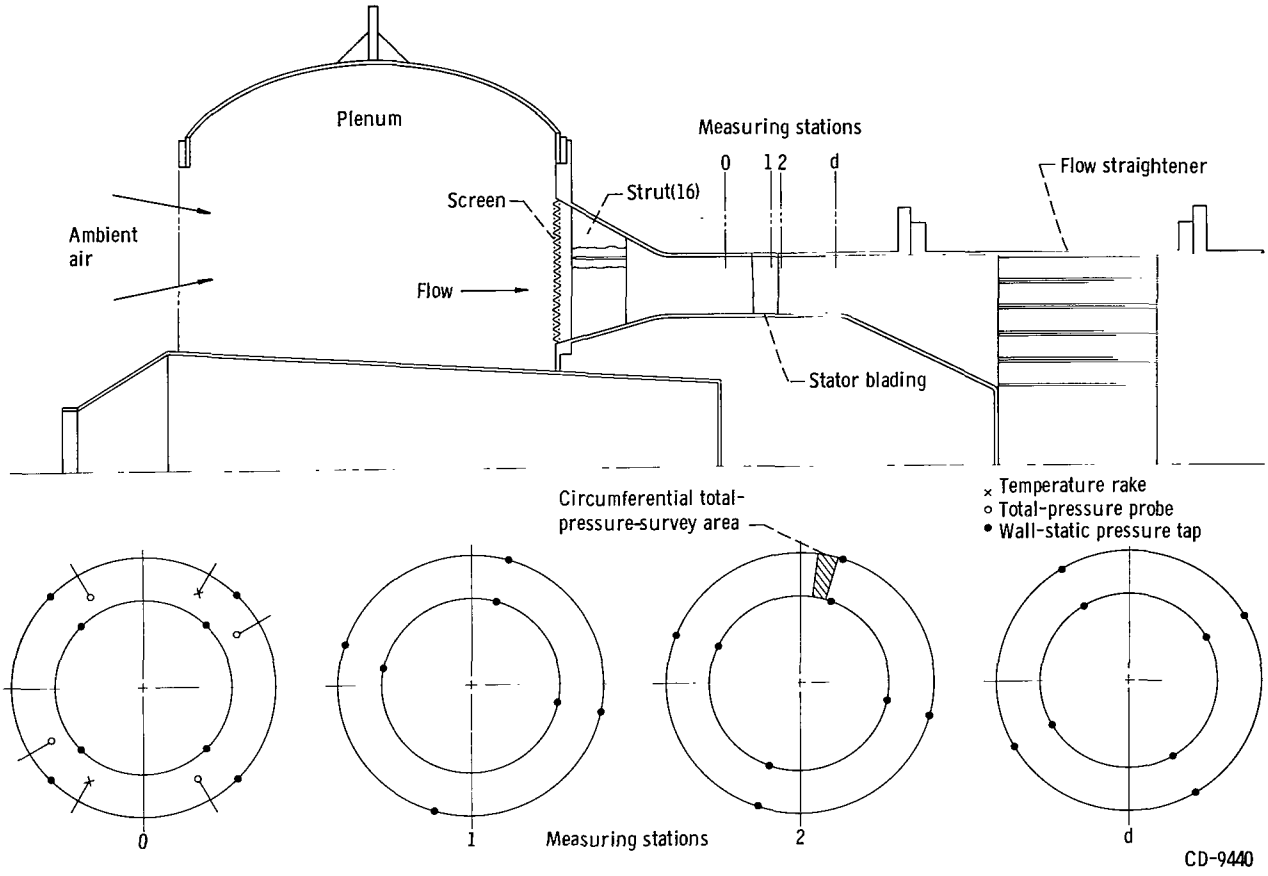

Figure 1. - Schematic diagram of turbine stator assembly and upstream view of instrumentation.

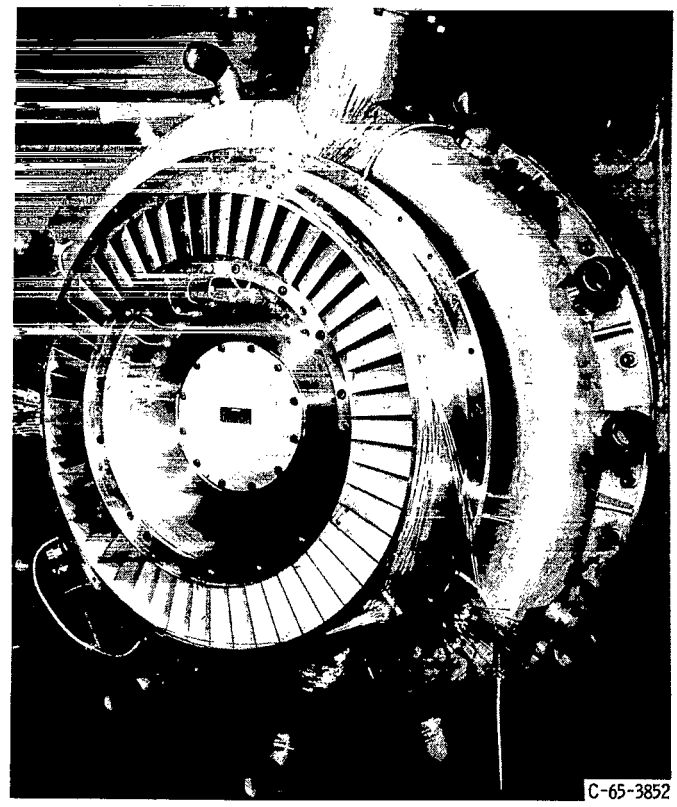

Figure 2. - Stator assembly.

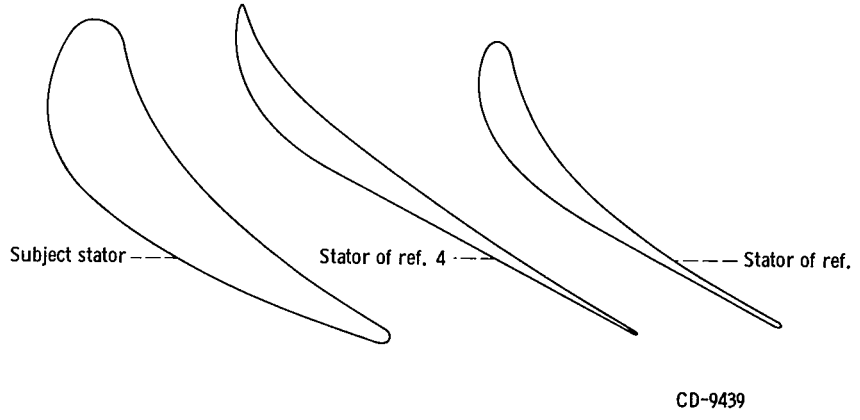

Figure 3. - Mean-section blade profiles of subject and reference stators.

located radially on centers of equal annular area. Four Kiel-type total-pressure probes were used to measure inlet total pressure. In addition, four static-pressure taps were located on both the inner and outer walls around the annulus at the inlet measuring station. Similar static-pressure-tap configurations were provided at the stator throat and exit (stations 1 and 2, respectively (see figs. 1 and 4)) as well as the downstream measuring station (station d) located about $2\frac{1}{2}$ blade chords behind the blade row. Of the taps at station 2, one inner-wall tap and one outer-wall tap were located at the center of the projected outlet flow passage adjacent to one of the survey passages (fig. 4).

Radial and circumferential total-pressure survey measurements were made about 0.005 inch (0.013 cm) downstream of the stator blade trailing edge, over a span encompassing two complete blade wakes (fig. 4). A calibrated total-pressure probe installed in an actuator permitted radial probe travel, with the sensing element oriented and fixed at an experimentally obtained average blade-exit flow angle. The actuator, in turn, was mounted on a saddle, which was lapped to the turbine casing, and driven circumferentially by a remotely controlled variable-speed motor through a rack and pinion. The probe-actuator-saddle assembly is shown in figure 5, with an enlargement of the probe sensing elements. Two tubes were required in order to obtain measurements at the inner and outer walls. The sensing end of both tubes was constructed of 0.012-inch (0.030-cm) tubing with a 0.006-inch (0.015-cm) inside diameter. Each probe was insulated and provided with an electrical signal to locate the probe with respect to the turbine inner and outer walls.

The length of the sensing portion of the total-pressure probe (about 1.2 in. (3.05 cm)) was necessitated by the combination of flow angle and the fact that the probe stem was located about 1/2 inch (1.27 cm) behind the blade trailing edge (see fig. 4). The latter dimension was arbitrarily selected in an effort to minimize probe-blockage effects on flow.

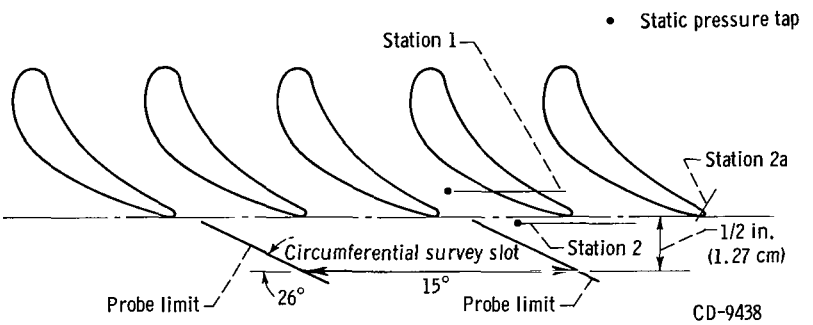

Figure 4. - Schematic presentation of circumferential total-pressure-survey probe travel at stator hub and proximal throat and blade-exit static-pressure taps.

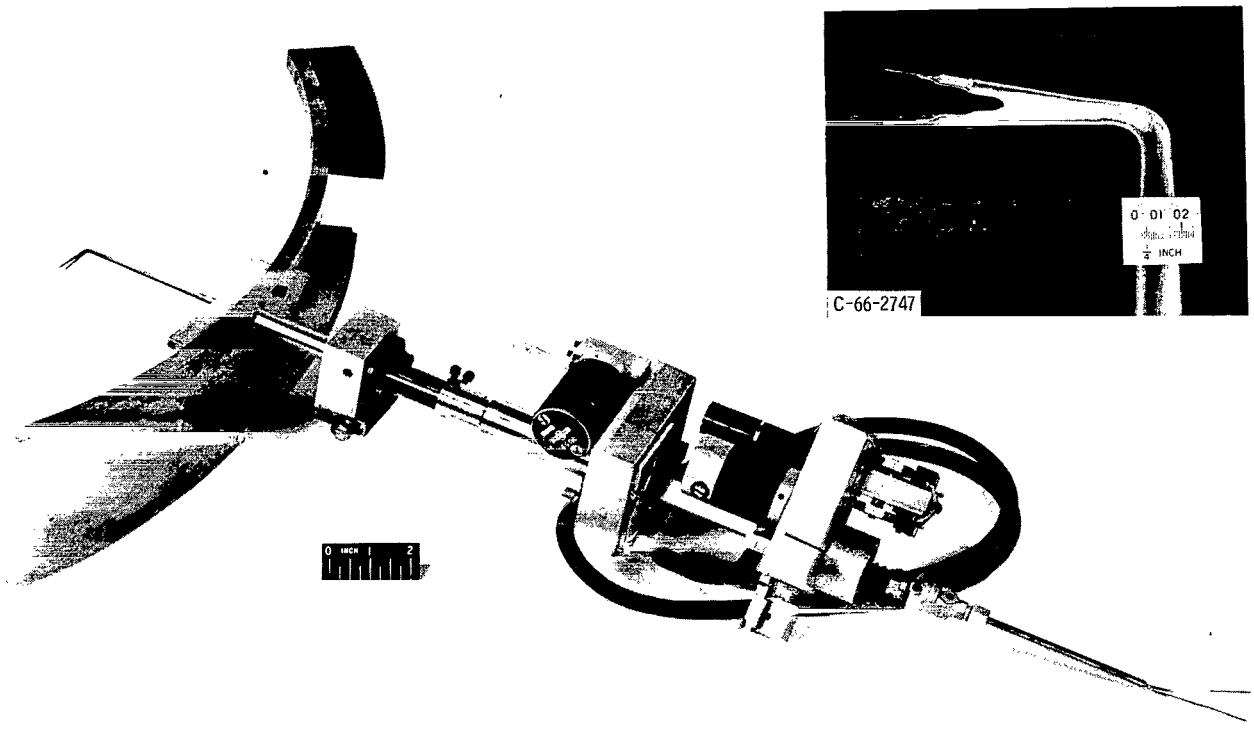

Figure 5. - Total-pressure-survey probe assembly.

TEST PROCEDURE

Preliminary tests were conducted to determine if circumferential pressure gradients occurred when the total-pressure probe was in the air stream. When conducting these tests, the downstream hub-static pressure, as established by one of the taps at station d (see fig. 1), was maintained constant by controlling valves in the piping to the laboratory exhaust system. These tests showed that negligible circumferential gradients occurred at the inner and outer walls of the inlet and downstream stations. Accordingly, both the hub and tip wall taps at each of these two stations were individually manifolded. However, at the blade exit (station 2) and at the throat (station 1), the measured pressures in the flow passage adjacent to the surveyed blades (fig. 4) were significantly affected by both radial and circumferential probe position. These pressures were therefore measured individually during testing. All pressure taps were connected to calibrated transducers. The electrical outputs from these transducers were recorded on a punch-tape digitizer, as were the 10 thermocouple readings.

Ambient air was used at the inlet of the turbine for all tests. Four test points were selected to cover a range of flow. The downstream stator blade hub-static pressure at measuring station d was maintained constant for each test point to provide inlet-total-to downstream-static-pressure ratios corresponding to hub-downstream critical velocity ratios of 0.5, 0.7, 0.896 (design), and 1.1. At each pressure ratio, blade-inlet, blade-exit, and downstream measurements were taken along with the radial and circumferential total-pressure-drop survey data. Output from the total-pressure-survey probe was connected to one side of a differential pressure transducer, and the other side was connected to one of the Kiel-type inlet-total-pressure probes. These total-pressure-drop data were recorded intermittently as a function of circumferential location on the digitizer as well as continuously on an X-Y recorder. Typical circumferential total-pressure-drop data, taken near the mean radius, are shown in figure 6. Concomittant digitizer data were obtained at about 0.40° circumferential increments in the free stream, and 0.04° in the wake area. The frequency of digitizer data points was regulated by monitoring the X-Y recorder traces and varying the saddle - drive-motor speed accordingly. Circumferential traverses were made at some 27 different radii, with the majority concentrated near the hub and tip regions, where the pressure-drop measurements were greatly affected by boundary layer.

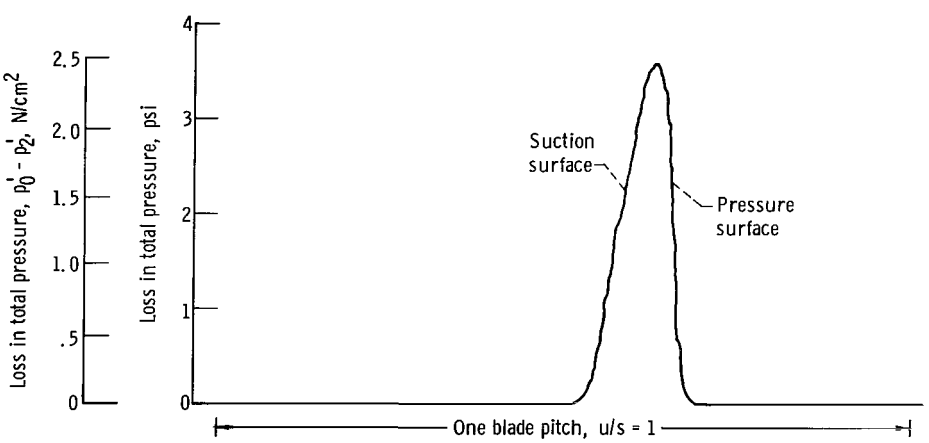

Figure 6. - Typical total-pressure-drop data at blade-exit near mean section. Ambient inlet conditions.

CALCULATION METHODS

Calculation Procedures

Experimental values of boundary-layer loss parameters and related loss coefficients were calculated from blade-inlet, blade-exit, and total-pressure-survey data. The general procedure in obtaining the experimental results was to first calculate values for thickness parameters at different radii, $\delta^*_{r,2}$, $\theta^*_{r,2}$, $\psi^*_{r,2}$, and $\xi^*_{r,2}$, at the blade-exit survey station just downstream of the trailing edge. These values of radial-sector parameters were next used to obtain annular-sector thickness parameters at the same station. Then values of mean-section (mean blade radius) and annular-sector blade-exit thickness parameters were used to calculate corresponding values of mean-section and annular-sector blade-exit kinetic energy loss coefficients and annular-sector after-mix kinetic energy loss coefficients, $\bar{e}_{2,m}$, $\bar{e}_{2,3d}$, and $\bar{e}_{3,3d}$, respectively.

Theoretical results were obtained from a method based on turbulent boundary-layer theory. The general procedure used in obtaining the results was to first calculate values for mean-radius blade-outlet thickness parameters. Once these values were known, essentially the same procedure as that used for calculating experimental results was employed for calculating theoretical values for mean-section and annular-sector loss coefficients.

The methods of references 3 to 6 were used as a guide for the experimental and theoretical calculations. For convenient referral, the methods, as used herein, are outlined in appendixes B and C. Appendix B pertains to the calculation of experimental results, and appendix C pertains to theoretical results.

Procedure Used in Predicting Performance of Reference Blading

In examining the effect of profile thickness and solidity on stator performance, the performance of stators of more conventional design was needed as a basis for comparing the performance of the subject stator configuration. The loss characteristics of two different stator configurations with thinner blade profiles and different solidities than the subject stator were previously investigated. The results are reported in references 4 and 5. However, the reference stators had blading of different chord length, radial height, and turning angle than the subject blading, and, therefore, the results cannot be directly compared.

In order to make the results comparable, the experimental performance of the referenced stators was corrected to the performance of stators with blading of the same chord length, radial height, and turning angle as the subject stator. The calculation

methods of appendixes B and C were used to make these corrections as described in the remaining paragraphs of this section.

Theoretical free-stream surface-velocity distributions around the mean section of the reference blading at specified inlet and exit conditions are available from reference 5 and 7. Stream filament theory shows that, with given conditions of pressure and temperature at the inlet and exit of the blading, the free-stream surface-velocity distribution around bladings with geometrically similar flow passages is the same. Bladings with geometrically similar cross-sectional flow passages must also have geometrically similar profiles and the same solidity.

Based on the information in the previous paragraph and the blade-surface velocity distribution of either reference 5 or 7, the method of appendix C was used to calculate theoretical values of mean-section boundary-layer thickness for two sets of geometrically similar blading, one with chord length equal to the reference set, the other with chord length equal to the subject set.

Theoretical values of mean-section boundary-layer thickness were then known for the reference blading and for the blading with chord length equal to the subject blading. With the assumption that small differences in turning angle (about 5°) have negligible effect on blade-surface-velocity distribution, the method of appendix B was then used to calculate values of mean-section and annular-sector loss coefficients for two stators with geometrically similar blade-surface-velocity distributions, one with chord, height, and turning angle equal to the reference blading, the other with chord, height, and turning angle equal to the subject blading. When the values of loss coefficients for the two stators were known, percentile differences in these loss coefficients were applied to the experimentally determined loss values of the reference stators to predict the test performance of stator blades with thinner profiles and different solidities than the subject blading, but with the same radial height, chord length, and turning angle as the subject blading.

BASIS OF RESULTS

Using the methods described to obtain experimental values of blade-exit loss quantities at particular radii requires knowledge of the free-stream conditions corresponding to the loss. The free-stream conditions for this investigation were obtained from measured blade-exit wall-tap static pressures and an assumed radial distribution of blade-exit static pressures. The free-stream conditions at blade exit varied with loss at each of the hub-section critical velocity ratios investigated. An investigation of the effect on experimental loss coefficients of differences in blade-exit static pressures resulting from probe blockage and from two different assumptions for radial pressure distribution is reported in appendix D. From the results of this investigation, it was concluded that values of loss coefficients for the subject stator above design hub-section critical vel-

ocity ratio of 0.896 would not be considered because above this critical velocity ratio the free-stream conditions corresponding to the loss are too uncertain. It was also concluded that, since the effect on loss coefficients of the two radial pressure distributions considered is relatively small, a linear radial pressure distribution would be used in order to be consistent with results for the reference stators. Since the blade losses were measured with the flow obstructed by the probe, the losses reported herein are correspondingly based on free-stream conditions with obstructed flow. Mean-section flow conditions were found to be representative of average flow conditions in the annular sector and were therefore used for average flow conditions when calculating annular-sector results. Stator performance results are reported as a function of ideal after-mix critical velocity ratio at the blade mean section. As a result of the selection of blade-exit conditions, the mean-section ideal after-mix critical velocity ratios (corresponding to test-point hub critical velocity ratios of 0.5, 0.7, 0.896, and 1.1) are 0.486, 0.664, 0.832, and 0.921, respectively.

When reporting experimental values of stator loss from annular-sector data, the end-wall loss from the inlet plenum to the face of the stator should not be charged to the stator itself. Therefore, experimental values of annular-sector losses reported herein have been corrected to exclude this loss. The entrance loss for the subject stator was experimentally obtained by applying total-pressure-loss data from radial surveys at the inlet station in the calculation methods of appendix B. This loss is quite small, equivalent to a pressure loss of about 0.05 percent of the inlet total pressure. Inlet end-wall loss was not required for the stator of reference 5 since the results reported are based on mean-section data only; annular-sector results for the stator of reference 4 have been corrected for inlet loss as described in the reference.

RESULTS AND DISCUSSION

The results of this investigation, based on considerations of the preceding discussion, are presented in three sections. The first section presents experimental results for the subject stator including annular variations in total-pressure ratio, variations of loss parameters with radius, and the variation of kinetic energy loss coefficients with Mach number. In the second section, a comparison of mean-section experimental and analytical kinetic energy loss coefficients for the subject stator and one of the reference stators is presented. A similar comparison of annular-sector results is also presented for the subject stator. In addition, trailing-edge loss is discussed. The last section is a comparison between experimentally based values of mean and annular-sector kinetic energy loss coefficients for the subject stator and two reference stators that have thinner profiles and different solidities than the subject stator.

Experimental Results

Figure 7 shows the annular variations in total-pressure ratio for the subject stator which were obtained from circumferential survey data at the four critical velocity ratios investigated. These results give some indication that the stator performed well, since the loss regions do not extend far into the free-stream area. The experimental results at station 2 were obtained from survey data measured downstream of the blade trailing edge and, therefore, must include not only the blade-surface and end-wall friction losses, but also the trailing-edge pressure loss.

Blade row losses are treated herein as a loss in kinetic energy by the use of kinetic energy loss coefficients. Kinetic energy loss coefficients $\bar{e}$ express the loss in kinetic energy as a decimal part of the ideal kinetic energy of the actual flow at the station corresponding to the loss. (Efficiency, on a kinetic energy basis, may be obtained by subtracting these coefficients from 1.) Kinetic energy loss coefficients are dependent on displacement thickness parameters δ^* and momentum thickness parameters θ^* at blade outlet. The displacement thickness parameter expresses the loss in flow as a decimal part of the ideal flow without blockage, and the momentum thickness parameter expresses the loss in momentum as a decimal part of the momentum of the ideal flow without blockage. The radial variation of these thickness parameters for the subject stator is shown in figure 8 at the four critical velocity ratios investigated. At radii near the inner and outer walls, the results show the expected large variations in loss caused by a combination of blade-surface, end-wall, and trailing-edge losses. At radii removed from the end-wall region, the loss also varies to some degree with radius. The trend of the variation may be generally described as showing increased loss with radial distance from a location which changes from a radius near the blade mean section at the higher critical velocity ratios (fig. 8(d)) to a radius nearer the hub section at lower critical velocity ratios (fig. 8(a)). This trend apparently results from the variation of blade loading with radius caused by decreasing blade solidity with increasing radius. In reference 2, experimental values of blade-loading diagrams are presented for the hub, mean, and tip sections of the subject blading at design critical velocity ratio. These diagrams indicate that the subject blading was too lightly loaded at the hub section, well loaded at the mean section, and too heavily loaded at the tip section. Blading which is too lightly loaded has excess friction loss caused by too large a ratio of surface area to flow area, and blading which is too highly loaded has excess loss caused by too large diffusion. Therefore, from blade-loading considerations, the loss trend with radius near design critical velocity ratio shown in figure 8 can be explained.

The change in radial location of minimum loss from a radius near the mean section at design critical velocity ratio to a radius nearer the hub section at lower critical velocity ratios can also be explained by blade-loading considerations. At reduced critical

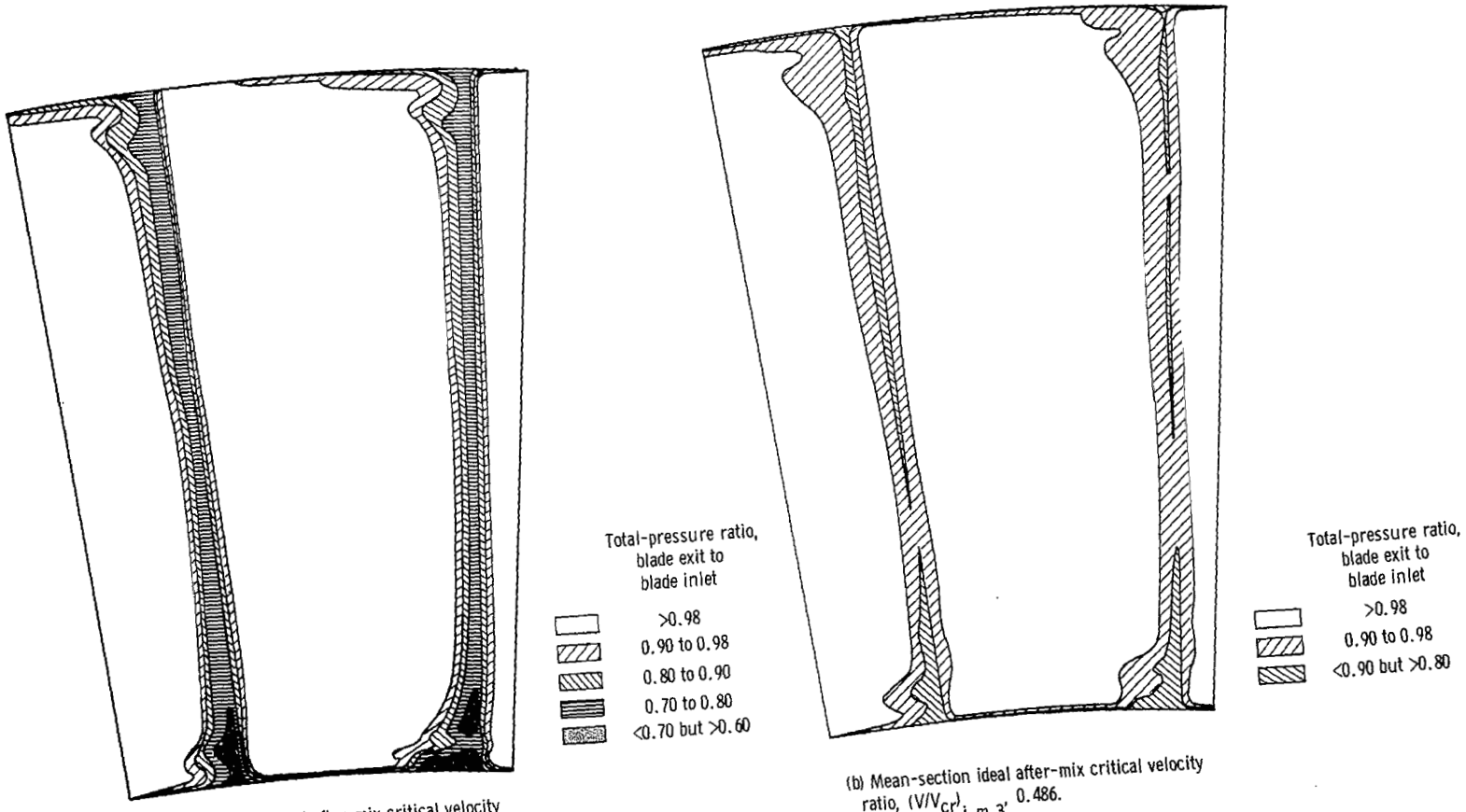

(a) Mean-section ideal after-mix critical velocity ratio, $(V/V_{cr})_{i,m,3}$, 0.832.

(b) Mean-section ideal after-mix critical velocity ratio, $(V/V_{cr})_{i,m,3}$, 0.486.

Figure 7. - Contours of total-pressure ratio from annular surveys.

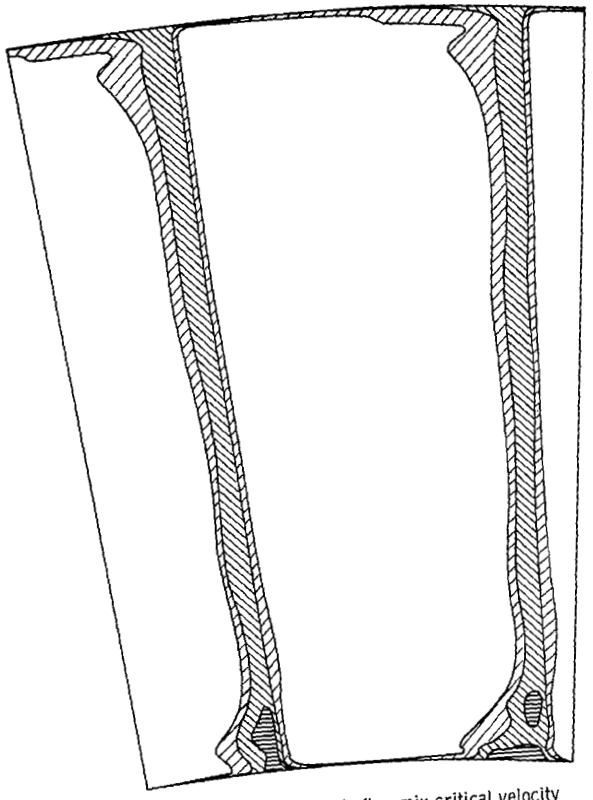

(c) Mean-section ideal after-mix critical velocity ratio, $(V/V_{cr})_{i,m,3}$, 0.664.

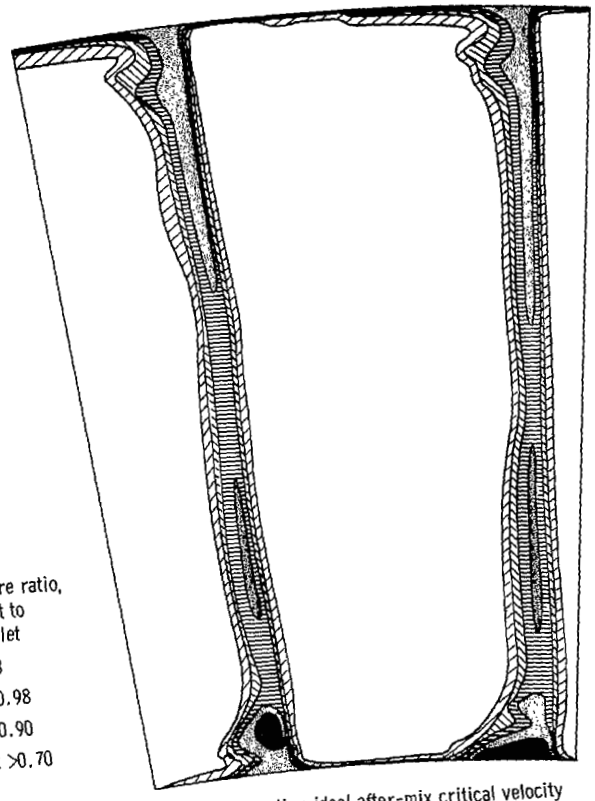

(d) Mean-section ideal after-mix critical velocity ratio, $(V/V_{cr})_{i,m,3}$, 0.921.

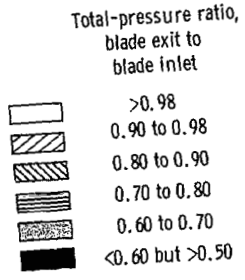

Figure 7. - Concluded.

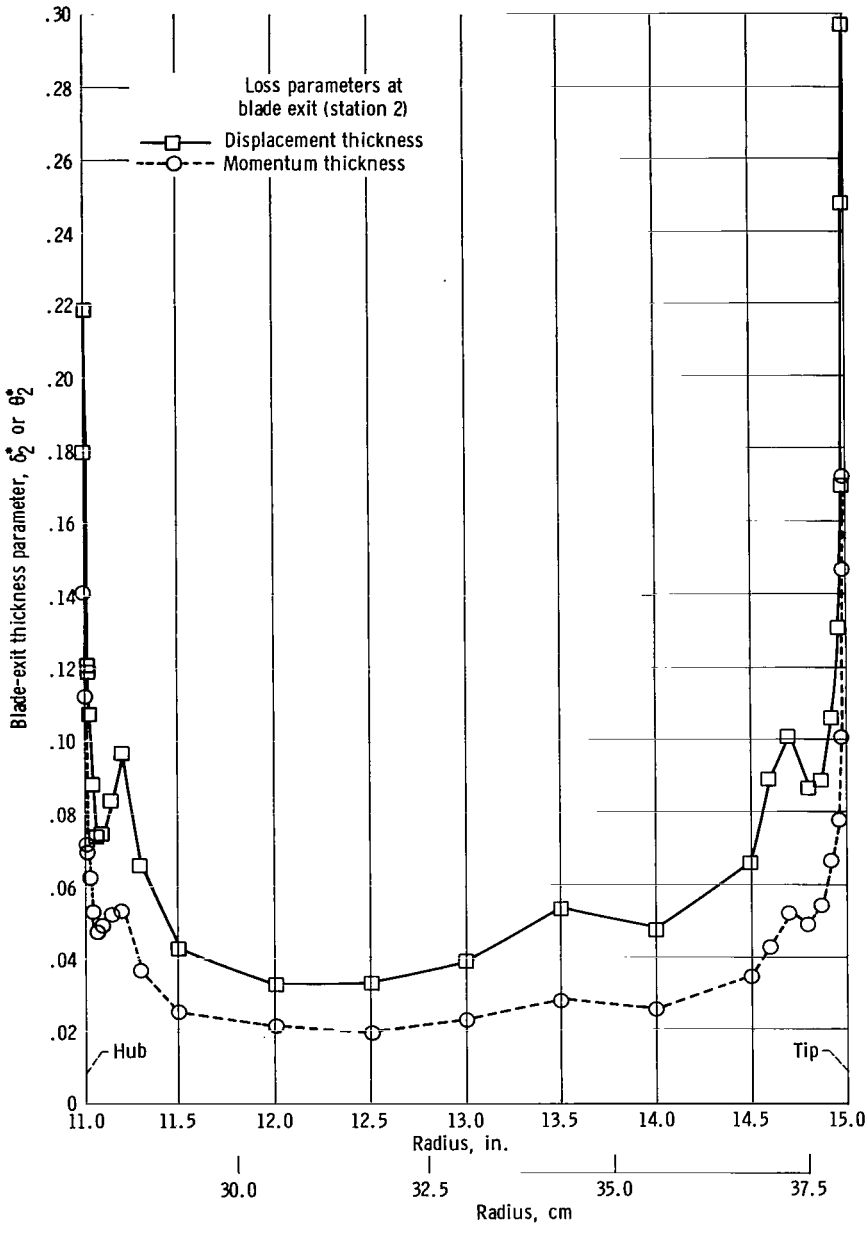

(a) Mean-section ideal after-mix critical velocity ratio, $(V/V_{cr})_{i,m,3}$, 0.486.

Figure 8. - Variation in blade-exit thickness parameters with radius.

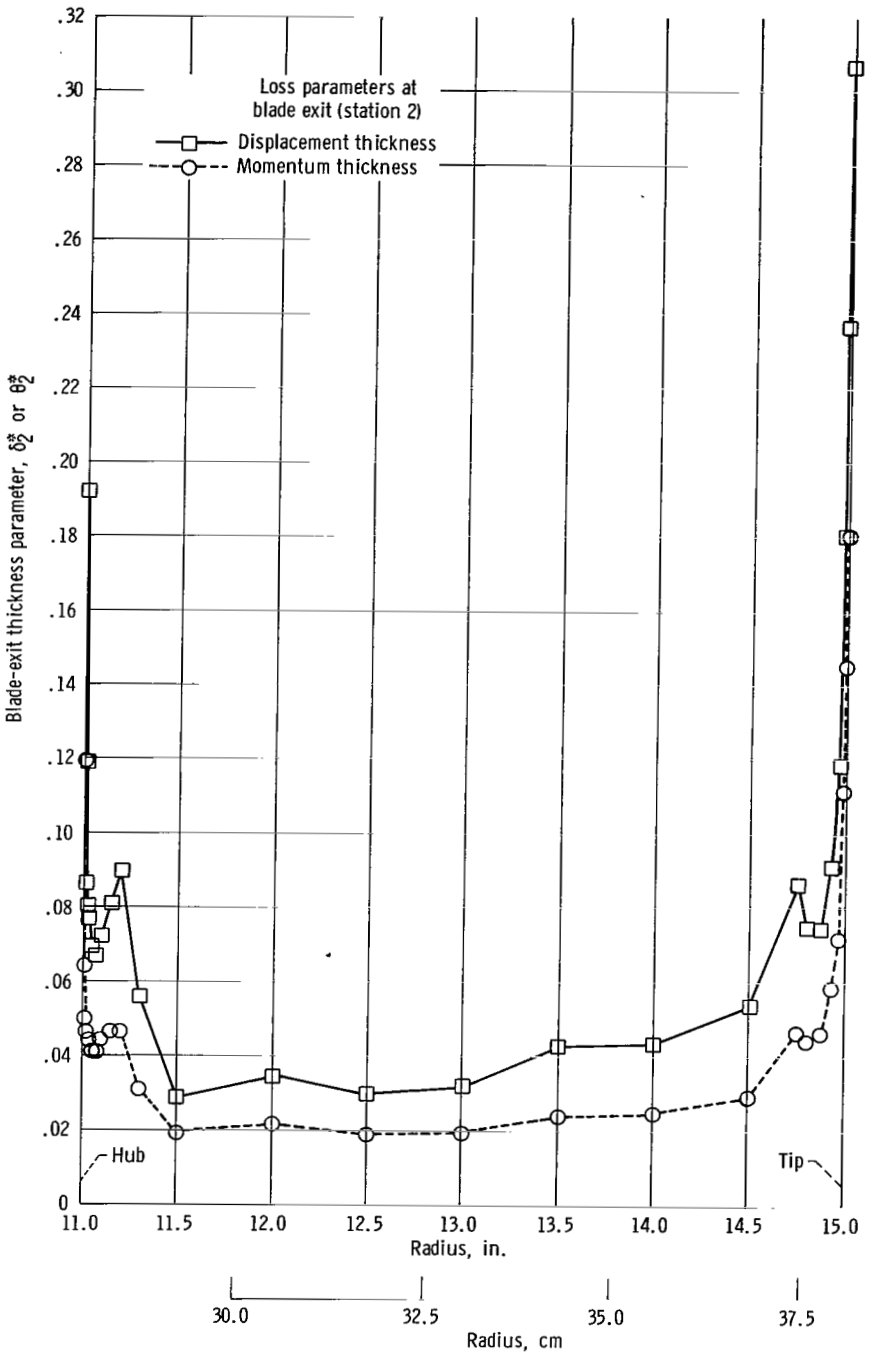

(b) Mean-section ideal after-mix critical velocity ratio, $(V/V_{cr})_{i,\,m,\,3'}$ 0.664.

Figure 8. - Continued.

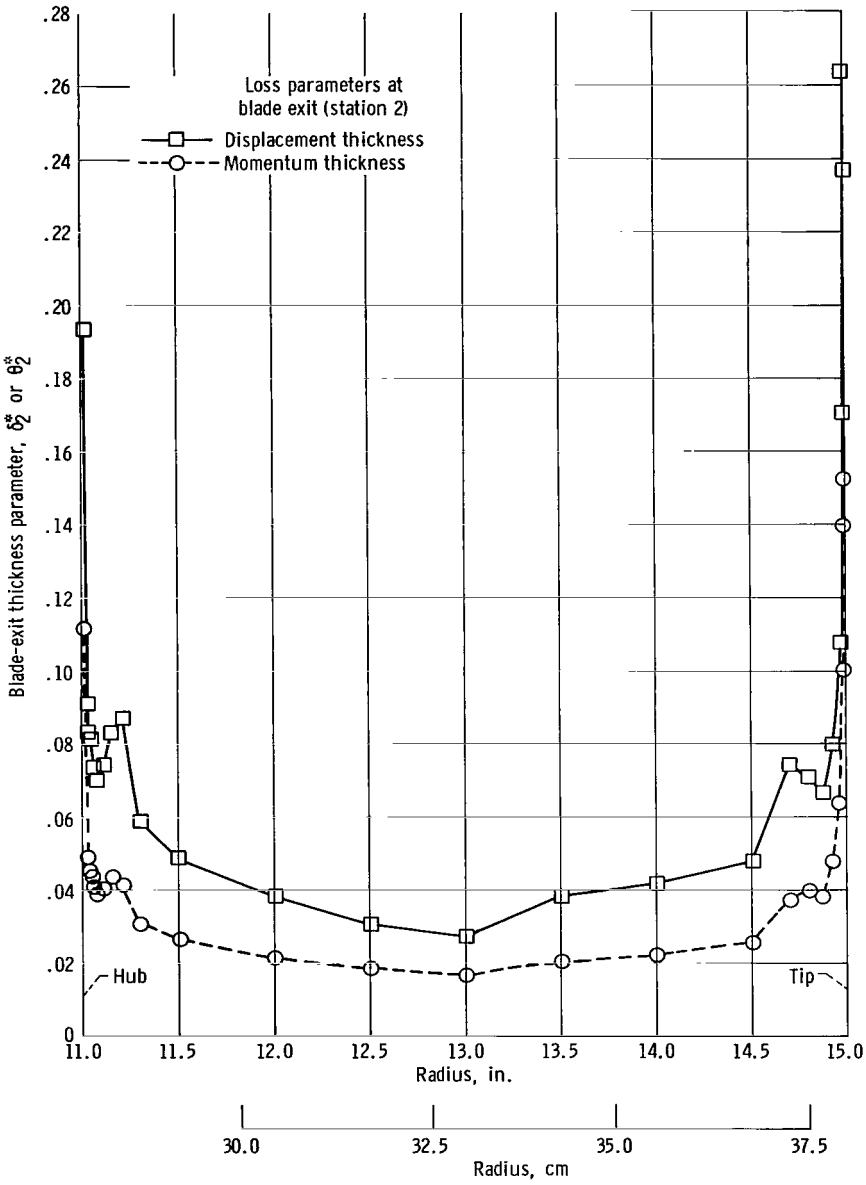

(c) Mean-section ideal after-mix critical velocity ratio, $(V/V_{cr})_{i, m, 3'}$ 0.832.

Figure 8. - Continued.

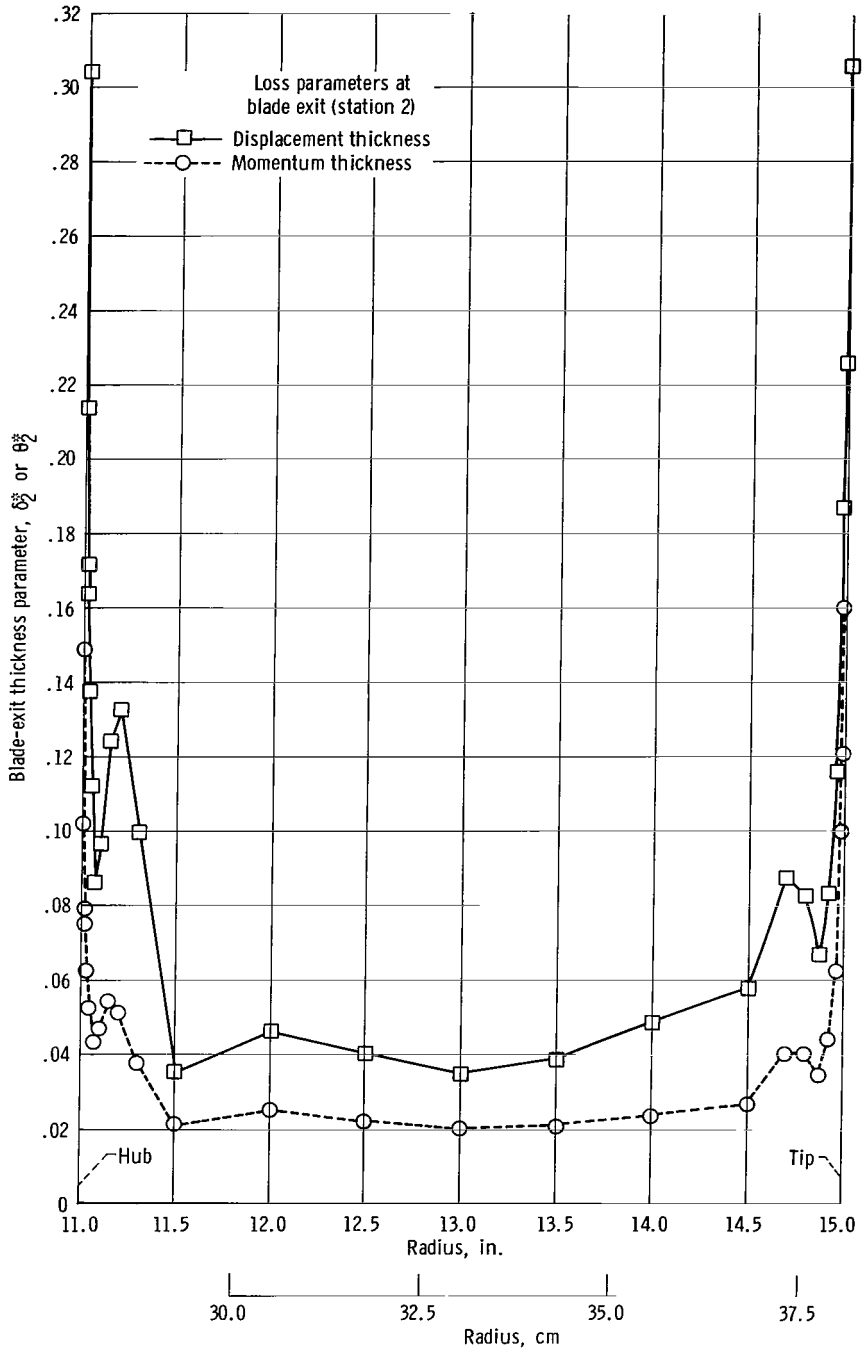

(d) Mean-section ideal after-mix critical velocity ratio, $(V/V_{cr})_{i,m,3'}$ 0.921.

Figure 8. - Concluded.

velocity ratios, the fluid acceleration in the channel is reduced. Reduced fluid acceleration tends to increase diffusion, so that higher blade solidities are required than with high fluid acceleration to maintain a proper balance between friction and diffusion losses. Blading with too high solidity at high critical velocity ratios would therefore have improved performance at reduced critical velocity ratios, whereas the performance of blading with too low solidity at high critical velocity ratios would be poorer at reduced critical velocity ratios. The subject blading at design critical velocity ratio appears to have too high solidity at the hub section and too low solidity at the tip section; consequently, the performance at the hub section is improved at lower Mach numbers and the performance of the tip section is made poorer. This results in a shift in minimum loss from the mean radius at design critical velocity ratio to a radius nearer the hub section at lower critical velocity ratios.

Experimentally obtained values of kinetic energy loss coefficients for the subject stator are shown in figure 9 over the range of critical velocity ratios being considered. The lower loss-coefficient curve in figure 9 shows values of mean-section blade-exit kinetic energy loss coefficients $\bar{e}_{2,\,m}$ which include the loss in kinetic energy due to blade-surface friction and trailing-edge loss at the blade-mean section. The middle curve shows values of annular-sector blade-exit kinetic energy loss coefficients $\bar{e}_{2,\,3d}$ which include the loss in kinetic energy due to surface friction of the complete blade, pressure loss of the whole trailing edge, and friction of the end walls. The upper curve

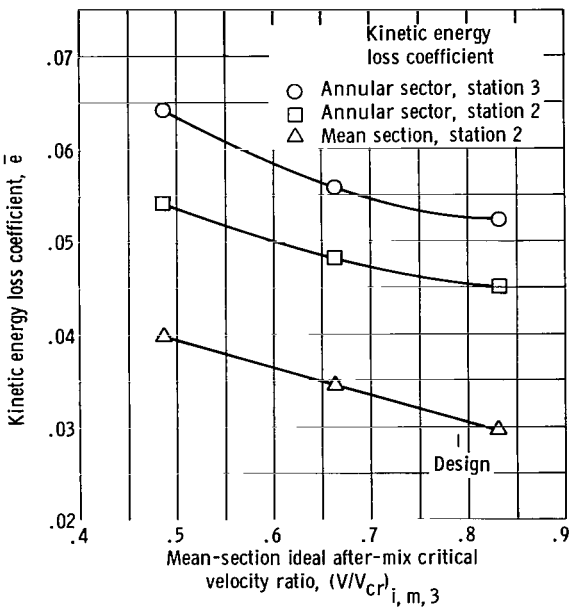

Figure 9. - Variation of kinetic energy loss coefficients for subject stator with after-mix critical velocity ratio (based on experimental data).

of overall blade row loss shows values of annular-sector after-mix kinetic energy loss coefficients $\bar{e}_{3,\,3d}$ which include the loss shown by the middle curve, and in addition, the mixing loss due to momentum exchange between the free-stream fluid and the lower velocity fluid from the loss regions.

The curves of experimental loss coefficients in figure 9 show a trend of decreasing loss with increasing velocity. This trend would be expected because of both Reynolds number and blade-loading effects. The upper curve shows the values of overall kinetic energy loss coefficients of the subject stator to vary from 0.064 at a critical velocity ratio of 0.486 to about 0.053 at design critical velocity ratio of 0.790 and higher.

The contributions of some of the separate losses to the overall blade row loss are also indicated by figure 9. Comparing the values of the upper and lower curves shows that if the surface-friction and trailing-edge losses at the blade mean section were representative of the loss of the total blade, these losses would contribute only about 60 percent to the overall loss. The difference between the lower two curves, when compared to the upper curve, indicates that end-wall losses, together with blade losses differing from those at the mean section, contributed about 25 percent to the overall blade row loss. And finally, the difference between the upper two curves indicates that mixing loss contributed about 15 percent to the overall blade row loss.

Comparison of Experimental and Analytical Results

Mean-section comparison. - Because surface-friction loss at the blade mean section is commonly considered the basic loss of the blade row, a comparison was made between experimental and analytical values of this loss. However, values of this loss cannot be directly compared because the experimental losses at the blade mean section include both surface-friction and trailing-edge losses, and the experimental trailing-edge loss could not be determined from the measured data.

Since experimental values of mean-section blade-surface-friction loss could not be obtained for comparison with analytical values, analytical values of mean-section blade-surface-friction loss plus trailing-edge loss were determined, and these values were compared with the corresponding experimental values. Figures 10(a) and (b) present a comparison of experimental and analytical values of these losses in terms of kinetic energy loss coefficients for the subject blading and the blading of reference 5, respectively. Good to excellent agreement is shown between these analytical and experimental mean-section results. At design mean-section critical velocity ratio for the subject blading, the difference between experimental and analytical mean-section kinetic energy loss coefficients was about 0.002 for the subject blading and about zero for the reference blading. The results shown in figures 10(a) and (b) are not for comparable stators, since

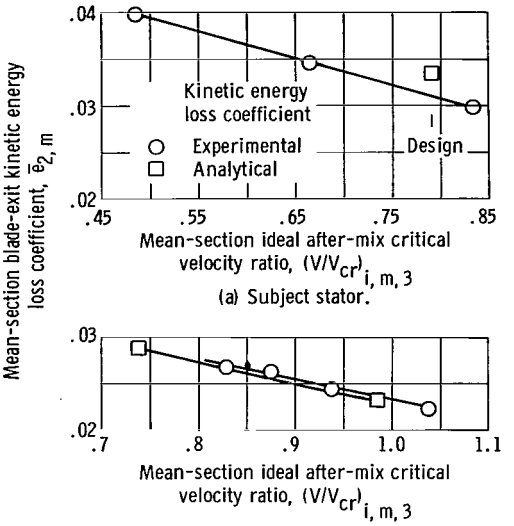

Figure 10. - Comparison of analytical and experimental mean-section blade-exit kinetic energy loss coefficients.

the radial height, chord length, and turning angle of the two stators are different.

The analytical values of blade-surface-friction loss and trailing-edge loss shown in figure 10 were determined from the methods of references 5 and 6, respectively. Another method for determining trailing-edge loss is included in reference 3. The method of reference 3 treats trailing-edge loss in its simplest concept as the loss due to sudden enlargement in flow area. This treatment of the loss assumes that only the axial component of flow is affected by the loss and neglects the effects of trailing-edge geometry and boundary-layer thickness at the blade trailing edge which would be expected to influence the loss. In comparison, the method of reference 6 treats the loss more comprehensively. It is a semi-empirical method based on boundary-layer theory and a collection of experimental data of losses resulting from flow around the trailing edge of airfoils and across overlapped sheet-metal joints with different edge geometries (i.e., square, rounded, etc.). In reference 6 values of loss calculated by the method are shown to agree well with experimental values of loss for a wide range of boundary-layer conditions, trailing-edge thicknesses, and a variety of sheet-metal joints.

Values of trailing-edge loss for the subject blading and the blading of reference 5 obtained by the two methods are shown in figure 11. At design critical velocity ratio, the figure compares the trailing-edge loss required to obtain agreement between analytical and experimental results with the trailing-edge loss calculated by the two methods, both

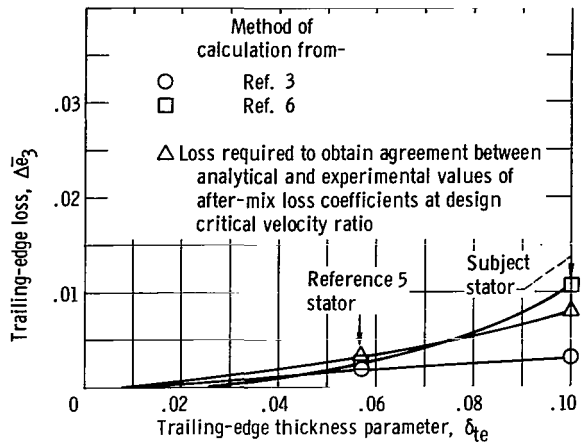

Figure 11. - Trailing-edge loss as function of trailing-edge thickness parameter at design critical velocity ratio.

for the subject blading and the blading of reference 5. These results show that the method of reference 6 better predicts the required loss for both bladings and also predicts a larger loss than that required for agreement with the subject blading. The loss and the difference in loss calculated by the two methods become appreciable at higher trailing-edge-thickness parameters, such as those encountered in cooled turbine blading. The loss indicated for the subject blading at 10 percent blockage is about 1 percent of the kinetic energy available to the stator.

For the reasons discussed in the preceding two paragraphs, analytical values of trailing-edge loss included in the results reported herein were obtained by the method of reference 6.

Annular-sector comparison. - Reference 4 presents a method, described in appendix C of this report, for predicting the annular-sector performance of stators from mean-section data, and also shows that the method satisfactorily predicted the annular-sector performance of the referenced blading. The principal assumption of the method is that the boundary-layer momentum thickness at the blade mean section is representative of the total blade surface and the inner and outer walls.

In figure 12, after-mix values of annular-sector performance for the subject blading predicted by the reference method are compared with values of annular-sector performance obtained from radial integration of experimental data. The upper curve of figure 12, then, is the same as the upper curve of figure 9. These results show the annular-sector loss coefficients obtained from annular data to be significantly larger than the

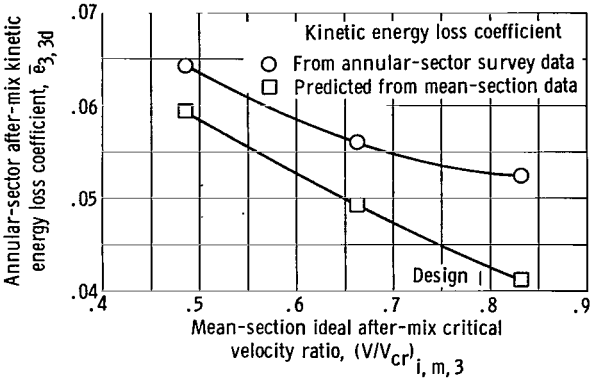

Figure 12. - Comparison of annular-sector after-mix loss coefficients for subject stator predicted from mean-section data with those obtained from annular-sector data.

predicted loss coefficients over the range of critical velocity ratios considered. The experimental coefficient of 0.053 based on annular-sector data is 0.010 greater than the predicted value of 0.043 (about 23 percent) at design critical velocity ratio. This disagreement was not unexpected. As discussed with respect to figure 8, because of blade-loading considerations, the experimentally obtained momentum thickness at the blade mean section of the subject blading is not representative of the total blade as assumed in the prediction method.

Comparison with Stators of Different Blade Profile Thicknesses and Solidities

The results for the subject stator were compared to similar results for two other stators with blading of thinner profiles and different solidities than the subject blading to examine the effect of blade profile thickness and solidity on stator performance. As discussed in CALCULATION METHODS, the results for the stators of references 4 and 5 were corrected for differences in radial height, chord length, and turning angle between the subject and reference stators in order to compare the results on an equivalent basis. Such corrections appear reasonable. The method of reference 5 for predicting blade-surface-friction loss, which is directly dependent on chord length and turning angle, together with the method of reference 6 for predicting trailing-edge loss, has been shown by the results of figure 10 to predict reasonably well the experimental mean-section performance of the two bladings considered. The method of reference 4 for predicting annular-sector loss from mean-section data, which is dependent on radial height, has been shown by the results of that reference to satisfactorily predict the experimental annular-sector performance of the reference stator. A comparison of mean-section

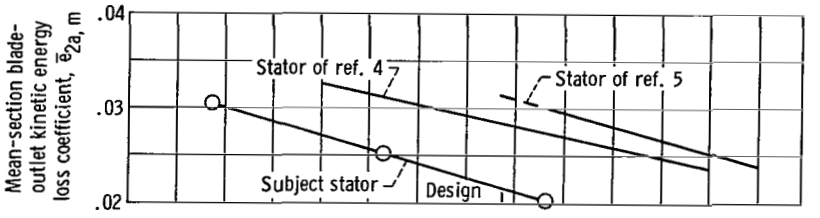

(a) Mean-section blade-outlet kinetic energy loss coefficient.

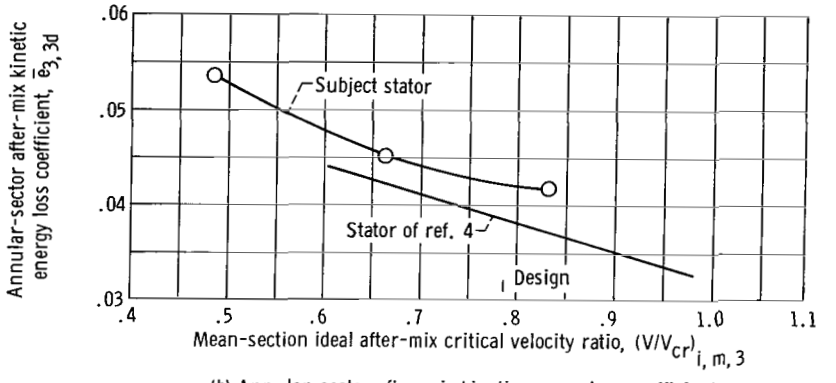

(b) Annular-sector after-mix kinetic energy loss coefficient.

Figure 13. - Comparison of performance of subject stator with predicted performance of reference stators. (Results shown exclude trailing-edge loss from method of ref. 6, see fig. 11.)

blade profiles for the subject and reference blading was shown in figure 3; the profile of the subject blading was thick relative to the profiles of the reference bladings. A comparison of mean-section solidities of the subject blading with the two reference bladings shows a mean-section solidity of 1.39 for the subject blading, 1.41 for the blading of reference 4, and 1.77 for the blading of reference 5. The solidity of the subject blading is therefore about the same as that of the blading of reference 4 but considerably lower than the solidity of the blading of reference 5.

In figures 13(a) and (b), the experimental performance results for the subject stator are compared on an equivalent basis with the two reference stators, which have thinner blade profiles and different solidities than the subject stator. The results shown in these figures have been adjusted to exclude the trailing-edge loss in order that the effects on stator performance of blade profile thickness and solidity could be considered separately.

In figure 13(a), a comparison of mean-section results for the subject blading with similiar results for the stator of reference 5 shows that the loss in kinetic energy caused by mean-section blade-surface friction was less for the subject stator than the estimated loss for the comparable stator with higher blade solidity and thinner profiles. The difference in mean-section kinetic energy loss coefficients was 0.010 at design critical

velocity ratio. These results suggest that the solidity of the stator of reference 5 may have been too high. A similar comparison of mean-section results for the subject stator with those for the stator of reference 4 shows that the loss in kinetic energy from mean-section blade-surface friction was also less for the subject stator than estimated for the comparable stator with thinner blade profiles and about the same solidity as the subject stator. The difference in loss coefficients was 0.007 at design critical velocity ratio.

In figure 13(b), annular-sector results for the subject stator are compared with similar results for the stator of reference 4. The reference results have been extrapolated to lower Mach numbers by using mean-section data from a single annular-sector test point. This extrapolation is justified by the results of reference 4 which show that annular-sector results for this stator could be well predicted from mean-section results. Figure 13(b) shows that for the stator with blading of the same chord length, radial height, and turning angle, the loss in kinetic energy caused by surface friction of the complete blade, surface friction of the end walls, and mixing was greater for the subject stator than that estimated for the stator of reference 4. The difference in loss coefficients was 0.004 at design critical velocity ratio. The results presented in figures 13(a) and (b), therefore, show the subject stator to have less surface-friction loss at the blade mean section than predicted for the stator of reference 4, but more surface-friction loss resulting from the total blade surface and end walls. These differences appear to result from blade-loading considerations.

No definite conclusions can be drawn from the results of this last section, but these results indicate that the increased profile thickness, excluding trailing-edge thickness, of the subject stator did not cause a significant penalty in performance, and that the mean-section blade solidity of the subject stator of 1.39 was not too low for good performance. These findings confirm in detail the results of reference 2, where it was indicated that from an overall viewpoint, the stator performed well.

SUMMARY OF RESULTS

An analytical and experimental investigation was made to determine the effect on turbine stator performance of the blade features of low solidity and large profile and trailing-edge thicknesses. Such features are desired for blading suitable for cooled turbine applications. Boundary-layer loss quantities and related loss coefficients were obtained. Loss coefficients for two other stators with thinner blade profiles and higher solidities than the subject blading were also predicted from referenced experimental data. In addition, analytical values of loss coefficients for the subject and one of the reference stators were computed. The results, based on both mean and annular sector data, are as follows:

1. At design mean-section critical velocity ratio of 0.790, the experimentally determined annular-sector after-mix kinetic energy loss coefficient for the subject stator was approximately 0.05. The curves of experimental loss coefficients as a function of critical velocity ratios show a trend of decreasing loss with increasing velocity. Such a trend would be expected because of Reynolds number and blade-loading effects.

2. A comparison of the experimental performance of the subject stator with the estimated performance of the two reference stators indicates that the performance of the subject blading was not significantly affected by increased profile thickness and that the mean-section solidity of the subject blading of 1.39 was not too low for good performance.

3. Good agreement was obtained between experimental and analytical mean-section results for the subject and one of the reference bladings. These results indicate that the large trailing-edge thickness of the subject stator (equal to about 10 percent blockage) caused a significant loss amounting to about 1 percent of the kinetic energy available to the stator.

4. At design mean-section critical velocity ratio, the annular-sector after-mix kinetic energy loss coefficient for the subject stator, obtained from annular-sector data, was 0.01 (about 23 percent) larger than the loss coefficient predicted from mean-section data. This rather poor agreement resulted from the experimentally determined momentum thickness at the mean section of the blading not being representative of the total blade surface and end walls as was assumed in the prediction method.

Lewis Research Center,
National Aeronautics and Space Administration,
Cleveland, Ohio, November 1, 1967,
720-03-01-35-22.

APPENDIX A

SYMBOLS

A	parameter equal to $[(\gamma - 1)/(\gamma + 1)](V/V_{cr})^2$
B	parameter defined in eq. (C8)
C	parameter defined in eq. (B17)
C_D	drag coefficient
c	blade chord length, ft (m)
c_D	independent drag coefficient
D	parameter defined in eq. (B18)
E	energy factor, ψ/θ, ψ^*/θ^*
$\bar{e}$	kinetic energy loss coefficient
H	form factor, δ/θ, δ^*/θ^*
h	blade radial height, ft (m)
K	parameter defined in eq. (C2)
n	exponent used in describing boundary-layer velocity profile, $(Y/\delta_{full})^n = V/V_{fs}$
P	pressure factor ξ/θ, ξ^*/θ^*
p	pressure, lb/ft^2 (N/m^2)
Re	Reynolds number
r	radius, ft (m)
s	blade spacing, ft (m)
t	blade trailing-edge thickness, ft (m)
u	distance in tangential direction, ft (m)
V	absolute gas velocity, ft/sec (m/sec)
Y	distance in direction normal to boundary-layer travel, ft (m)
z	distance along blade surface measured from forward stagnation point, ft (m)
α	flow angle measured from axial direction, deg
α_{st}	stagger angle measured from axial direction, deg
γ	ratio of specific heats
δ	displacement thickness, ft (m)
δ^*	displacement thickness parameter, $\delta_{tot}/s \cos \alpha$
δ_{full}	full boundary-layer height, ft (m)
δ_{te}	ratio of tangential component of trailing-edge thickness to spacing; trailing-edge thickness parameter, $t/s \cos \alpha_{2a}$
θ	momentum thickness, ft (m)
θ^*	momentum thickness parameter, $\theta_{tot}/s \cos \alpha$
μ	gas viscosity, lb/(ft)(sec) (kg/(m)(sec))
ρ	gas density, lb/ft^3 (kg/m^3)
ξ	pressure thickness, ft (m)
ξ^*	pressure thickness parameter, $\xi_{tot}/s \cos \alpha$
ψ	energy thickness, ft (m)

ψ^*	energy thickness parameter, $\psi_{tot}/s \cos \alpha$

Subscripts:

av	average free-stream conditions
corr	corrected to average free-stream conditions
cr	conditions at Mach 1
d	station downstream used for set point
fs	conditions at free stream or that region between blade wakes
h	blade hub section
i	ideal conditions corresponding to isentropic process
m	blade mean section
p	blade pressure surface
r	radius
s	blade suction surface
t	blade tip section
te	trailing edge
tot	sum of blade suction and pressure surface quantities
u	tangential component
x	axial component
z	distance along blade surface measured from forward stagnation point
0	station upstream of blade row
1	station at stator throat
2	station just downstream of stator trailing edge (blade exit)
2a	station just inside stator trailing edge (blade outlet)
3	station after complete mixing occurs
3d	three dimensional or annular sector

Superscript:

(')	total state

APPENDIX B

CALCULATION OF EXPERIMENTAL RESULTS

Calculation of Radial-Sector Loss Characteristics at Blade Exit (Station 2) Immediately Downstream of Trailing Edge

Values of radial-sector thickness parameters at station 2 were calculated from experimental pressure data by using equations (17a) to (17d) of reference 3 which are as follows:

$$\delta^*_{r,2} = 1 - \delta_{te} - \int_0^1 \left(\frac{\rho V}{\rho_{fs} V_{fs}}\right)_{r,2} d\left(\frac{u}{s}\right) \tag{B1}$$

$$\theta^*_{r,2} = \int_0^1 \left[1 - \left(\frac{V}{V_{fs}}\right)_{r,2}\right]\left(\frac{\rho V}{\rho_{fs} V_{fs}}\right)_{r,2} d\left(\frac{u}{s}\right) \tag{B2}$$

$$\psi^*_{r,2} = \int_0^1 \left[1 - \left(\frac{V}{V_{fs}}\right)^2_{r,2}\right]\left(\frac{\rho V}{\rho_{fs} V_{fs}}\right)_{r,2} d\left(\frac{u}{s}\right) \tag{B3}$$

$$\xi^*_{r,2} = \int_0^1 \frac{\left[1 - \left(\frac{p'_2}{p'_0}\right)_r\right]\left(\frac{\rho V}{\rho_{fs} V_{fs}}\right)_{r,2} d\left(\frac{u}{s}\right)}{1 - \left(\frac{p_2}{p'_0}\right)_r} \tag{B4}$$

where $p'_0 = p'_{fs}$.

To solve the preceding equations using experimental pressure data, it is necessary to relate the density and velocity-ratio functions to pressure functions. With the assump-

tion that the static pressure and the total temperature through the boundary layer are the same as in the free stream, these relations are

$$\left(\frac{\rho}{\rho_{fs}}\right)_{r,2} = \left(\frac{p'_2}{p'_0}\right)_r^{(\gamma-1)/\gamma} \tag{B5}$$

$$\left(\frac{V}{V_{fs}}\right)_{r,2}^2 = \frac{1 - \left(\frac{p_2}{p'_2}\right)_r^{(\gamma-1)/\gamma}}{1 - \left(\frac{p_2}{p'_0}\right)_r^{(\gamma-1)/\gamma}} \tag{B6}$$

Substituting the values of thickness parameters obtained from equations (B1) to (B4) in the following equations, values of the boundary-layer factors at station 2 were also calculated.

$$H_{r,2} = \left(\frac{\delta^*}{\theta^*}\right)_{r,2} \tag{B7}$$

$$E_{r,2} = \left(\frac{\psi^*}{\theta^*}\right)_{r,2} \tag{B8}$$

$$P_{r,2} = \left(\frac{\xi^*}{\theta^*}\right)_{r,2} \tag{B9}$$

When values of the blade-exit thickness parameters have been obtained, values of blade-exit kinetic energy loss coefficients may be calculated by using the following equation (ref. 3):

$$\bar{e}_2 = \frac{\theta_2^* E}{1 - \delta_2^* - \delta_{te}} \tag{B10}$$

The total pressure traces taken at measuring station 2 showed that fluid had filled the trailing-edge region. Therefore, the trailing-edge thickness term δ_{te} was omitted from equations (B1) and (B10) when calculating experimental values of displacement thickness parameter and kinetic energy loss coefficients corresponding to station 2.

Calculation of Annular-Sector Loss Characteristics by Radial Integration at Blade Exit (Station 2)

When the radial variation of blade-exit static pressure and average blade-exit free-stream flow conditions are known, the values of radial-sector displacement thickness parameters calculated from equations (B1) to (B4) for flow conditions at corresponding radii are easily corrected to values based on average flow conditions in the annular sector. Thus, in terms of density and velocity ratios at blade exit

$$\delta^*_{r,2,corr} = \delta^*_{r,2} \frac{(\rho V)_{fs,r,2}}{(\rho V)_{fs,av,2}} \tag{B11}$$

or in terms of pressure ratio at blade exit

$$\delta^*_{r,2,corr} = \delta^*_{r,2} \left(\frac{p_r}{p_{av}}\right)_2^{1/\gamma} \left[\frac{1 - \left(\frac{p_2}{p'_0}\right)_r^{(\gamma-1)/\gamma}}{1 - \left(\frac{p_2}{p'_0}\right)_{av}^{(\gamma-1)/\gamma}}\right]^{1/2} \tag{B12}$$

In a similar manner, other thickness parameters obtained for flow conditions at corresponding radii may be corrected to average flow conditions in the annular sector.

Once the radial variation of thickness parameters based on average flow conditions is known, annular-sector parameters are obtainable by integration. The equations of integration, which are either presented in reference 4 or which may be developed in a manner similar to that of the reference, are as follows:

$$\delta^*_{2,\,3d} = \frac{2\displaystyle\int_{r_h}^{r_t} \delta^*_{r,\,2}\left(\frac{p_r}{p_{av}}\right)_2^{1/\gamma}\left[\frac{1-\left(\frac{p_2}{p'_0}\right)_r^{(\gamma-1)/\gamma}}{1-\left(\frac{p_2}{p'_0}\right)_{av}^{(\gamma-1)/\gamma}}\right]^{1/2} r\,dr}{r_t^2\left[1-\left(\frac{r_h}{r_t}\right)^2\right]} \qquad \text{(B13)}$$

$$\theta^*_{2,\,3d} = \frac{2\displaystyle\int_{r_h}^{r_t} \theta^*_{r,\,2}\left(\frac{p_r}{p_{av}}\right)_2^{1/\gamma}\left[\frac{1-\left(\frac{p_2}{p'_0}\right)_r^{(\gamma-1)/\gamma}}{1-\left(\frac{p_2}{p'_0}\right)_{av}^{(\gamma-1)/\gamma}}\right] r\,dr}{r_t^2\left[1-\left(\frac{r_h}{r_t}\right)^2\right]} \qquad \text{(B14)}$$

$$\psi_{2,\,3d}^{*} = \frac{2\displaystyle\int_{r_h}^{r_t} \psi_{r,\,2}^{*}\left(\frac{p_r}{p_{av}}\right)_2^{1/\gamma}\left[\frac{1-\left(\frac{p_2}{p_0'}\right)_r^{(\gamma-1)/\gamma}}{1-\left(\frac{p_2}{p_0'}\right)_{av}^{(\gamma-1)/\gamma}}\right]^{3/2} r\,dr}{r_t^2\left[1-\left(\frac{r_h}{r_t}\right)^2\right]} \tag{B15}$$

Conditions at the blade-mean section were considered to be average conditions for these calculations.

When values of annular-sector blade-exit thickness parameters have been obtained, values of annular-sector blade-exit kinetic energy loss coefficients may be calculated by using equation (B10).

Calculation of After-Mix Loss Coefficients

The method of reference 3 was used to obtain the after-mix or overall loss coefficients. The necessary equations from the reference method for calculating overall kinetic energy loss coefficients are listed in the following equations. The required parameters for these equations were obtained as described in the preceding section.

$$A_{fs,\,2} = \left(\frac{\gamma-1}{\gamma+1}\right)\left(\frac{V}{V_{cr}}\right)_{fs,\,2}^{2} \tag{B16}$$

$$C = \frac{\left(1-A_{fs,\,2}\right)\frac{\gamma+1}{2\gamma} + \cos^2\alpha_2\left(1-\delta_2^{*}-\delta_{te}-\theta_2^{*}\right)\left(\frac{V}{V_{cr}}\right)_{fs,\,2}^{2}}{\cos\alpha_2\left(1-\delta_2^{*}-\delta_{te}\right)\left(\frac{V}{V_{cr}}\right)_{fs,\,2}} \tag{B17}$$

$$\left(\frac{V_u}{V_{cr}}\right)_3 = D = \left(\frac{V}{V_{cr}}\right)_{fs,2} \sin \alpha_2 \frac{\left(1 - \delta_2^* - \delta_{te} - \theta_2^*\right)}{\left(1 - \delta_2^* - \delta_{te}\right)} \tag{B18}$$

$$\left(\frac{V_x}{V_{cr}}\right)_3 = \frac{\gamma C}{\gamma + 1} - \sqrt{\left(\frac{\gamma C}{\gamma + 1}\right)^2 - 1 + \left(\frac{\gamma - 1}{\gamma + 1}\right) D^2} \tag{B19}$$

$$\left(\frac{\rho}{\rho'}\right)_3 = \left\{1 - \frac{\gamma - 1}{\gamma + 1}\left[D^2 + \left(\frac{V_x}{V_{cr}}\right)_3^2\right]\right\}^{1/(\gamma-1)} \tag{B20}$$

$$\left(\frac{\rho}{\rho'}\right)_{fs,2} = \left(\frac{p_2}{p_0'}\right)^{1/\gamma} \tag{B21}$$

$$\left(\frac{p_3'}{p_0'}\right) = \frac{\left(\frac{\rho V}{\rho' V_{cr}}\right)_{fs,2} \cos \alpha_2 \left(1 - \delta_2^* - \delta_{te}\right)}{\left(\frac{\rho V_x}{\rho' V_{cr}}\right)_3} \tag{B22}$$

$$\bar{e}_3 = \frac{\left(\frac{p_0'}{p_3'}\right)^{(\gamma-1)/\gamma} - 1}{\left(\frac{p_0'}{p_3}\right)^{(\gamma-1)/\gamma} - 1} \tag{B23}$$

As mentioned in the first section of this appendix, the trailing-edge term δ_{te} was omitted when calculating loss coefficients based on conditions at station 2. The equations of the section also apply for calculating after-mix loss coefficient based on conditions at station 2a.

APPENDIX C

CALCULATION OF THEORETICAL RESULTS

Calculation of Mean-Section Loss Characteristics at Blade-Outlet

Theoretical values of mean-section, blade-outlet, boundary-layer momentum thickness for the suction and pressure surfaces of the blades were calculated from a method based on turbulent boundary-layer theory presented in reference 5. The following equation, from the reference, relates momentum thickness to free-stream flow and boundary-layer quantities.

$$\theta_z = \frac{0.231}{\left[\left(\frac{\rho V}{\rho V_{cr}}\right)_{fs}\left(\frac{V}{V_{cr}}\right)_{fs}^{(1+H)}\right]_z}\left\{\int_0^z \frac{\left[\left(\frac{\rho V}{\rho' V_{cr}}\right)_{fs}\left(\frac{V}{V_{cr}}\right)_{fs}^{(1+H)}\right]^{1.268}\left(\frac{\mu}{\rho V}\right)_{fs}^{0.268} K\,dz}{10^{0.678(2n+1)}}\right\}^{0.7886} \tag{C1}$$

where

$$K = \left[1 - \left(\frac{\gamma - 1}{\gamma + 1}\right)\left(\frac{V}{V_{cr}}\right)_{fs,z}^{2}\right]^{0.467} \tag{C2}$$

Solving this equation at a given blade-outlet critical velocity ratio requires the following information:

(1) The variation of free-stream blade-surface velocity with blade-surface length

(2) The variation of boundary-layer velocity-profile exponent with blade-surface length

(3) The variation of boundary-layer form factor with blade-surface length

The theoretical variation of mean-section free-stream blade-surface velocity with blade-surface length was obtained from previously calculated stator design data. The variation of the velocity-profile exponent with blade-surface length was obtained by using the following equation from reference 5:

$$\frac{1}{n_z} = 2.6\ \mathrm{Re}_{fs,z}^{1/14} \tag{C3}$$

where $\mathrm{Re}_{fs,z}$ is free-stream Reynolds number at the surface length being considered. From the values of blade-surface velocity ratio and velocity-profile exponents, the variation of the form factor with blade-surface length was determined by using the following equation from reference 3:

$$H_z = \frac{\dfrac{1}{n_z + 1} + \dfrac{3A_{fs,z}}{3n_z + 1} + \dfrac{5A_{fs,z}^2}{5n_z + 1} + \cdots}{\dfrac{1}{(n_z + 1)(2n_z + 1)} + \dfrac{A_{fs,z}}{(3n_z + 1)(4n_z + 1)} + \dfrac{A_{fs,z}^2}{(5n_z + 1)(6n_z + 1)} + \cdots} \tag{C4}$$

where

$$A_{fs,z} = \left(\frac{\gamma - 1}{\gamma + 1}\right)\left(\frac{V}{V_{cr}}\right)_{fs,z}^2 \tag{C5}$$

Theoretical values of mean-section blade-outlet form factor were determined for the suction and pressure surfaces of the blades as part of the preceding calculations. In addition, theoretical values of the mean-section blade-outlet energy and pressure factors were also determined for the suction and pressure surface of the blading at design blade-outlet critical velocity ratio. The following equations derived in reference 3 were used to calculate values for these factors:

$$E = \frac{2\left[\frac{1}{(n+1)(3n+1)} + \frac{A_{fs}}{(3n+1)(5n+1)} + \frac{A_{fs}^2}{(5n+1)(7n+1)} + \ldots\right]}{\frac{1}{(n+1)(2n+1)} + \frac{A_{fs}}{(3n+1)(4n+1)} + \frac{A_{fs}^2}{(5n+1)(6n+1)} + \ldots} \tag{C6}$$

$$P = \frac{\frac{1 - \left(\frac{p}{p'}\right)_{fs}}{n+1} + \frac{A_{fs}\left[1 - \left(\frac{p}{p'}\right)_{fs} B\right]}{3n+1} + \frac{A_{fs}^2\left[1 - \left(\frac{p}{p'}\right)_{fs} \frac{B(B+1)}{2!}\right]}{5n+1} + \ldots}{n\left[1 - \left(\frac{p}{p'}\right)_{fs}\right]\left[\frac{1}{(n+1)(2n+1)} + \frac{A_{fs}}{(3n+1)(4n+1)} + \frac{A_{fs}^2}{(5n+1)(6n+1)} + \ldots\right]} \tag{C7}$$

where

$$B = \frac{2\gamma - 1}{\gamma - 1} \tag{C8}$$

and the value of the exponent n corresponds to that obtained from equation (C3) at blade-surface outlet conditions.

When mean-section values for momentum thickness and the boundary-layer factors for the suction and pressure blade surfaces are known, corresponding values for the total blade surface can be calculated as follows:

$$\theta_{tot} = \theta_s + \theta_p \tag{C9}$$

$$H_{tot} = \frac{H_s\theta_s + H_p\theta_p}{\theta_{tot}} \tag{C10}$$

$$E_{tot} = \frac{E_s\theta_s + E_p\theta_p}{\theta_{tot}} \tag{C11}$$

$$P_{tot} = \frac{P_s \theta_s + P_p \theta_p}{\theta_{tot}} \tag{C12}$$

Calculation of Annular-Sector Blade-Outlet Loss Characteristics From Mean-Section Data

Values of annular-sector blade-outlet momentum thickness parameters were predicted from previously obtained values of mean-section blade-outlet momentum thickness parameters by using the equations

$$\theta^*_{2a,\,3d} = \left[1 + \left(\frac{s \cos \alpha_{st}}{h}\right)_m\right] \theta^*_{m,\,2a} \tag{C13}$$

$$\theta^*_{m,\,2a} = \left(\frac{\theta_{tot}}{s \cos \alpha}\right)_{m,\,2a} \tag{C14}$$

from a method developed in reference 4. In deriving the above equation, the following assumptions were made in the reference method:

(1) A given blade configuration can be satisfactorily approximated by an equivalent blade of the same height which has constant cross section, spacing, and stagger angle equal to those at the mean-section of the given blade.

(2) The momentum thickness per unit surface at the mean section of the blade is representative of all the blade surface and the inner- and outer-wall surfaces.

When blade-outlet momentum thickness parameters and thickness factors are known, values of other mean-section and thickness parameters can be obtained from the thickness factor equations, by assuming that the annular-sector thickness factors equal the mean-section factors.

Calculation of After-Mix Loss Characteristics

Methods for calculating values of blade-exit and after-mix loss coefficients when values of specified parameters are known are presented in appendix B. These methods also apply to and were used for the calculation of theoretical loss coefficients.

Calculation of Trailing-Edge Loss By the Method of Reference 3

The boundary-layer thickness at blade outlet is the same for the same blading regardless of trailing-edge thickness; however, the thickness parameters at blade outlet are different since these parameters are related to the free-stream flow without blockage. Therefore, with trailing-edge thickness,

$$\delta^*_{2a} = \frac{\delta_{tot}}{s \cos \alpha_{2a}} \tag{C15}$$

and without trailing-edge thickness

$$\delta^*_{2a} = \frac{\delta_{tot}}{s \cos \alpha_{2a} - t} \tag{C16}$$

and similarly for the momentum thickness parameters at station 2a.

When values of displacement and momentum thickness parameters for the two bladings, one with and the other without trailing-edge thickness, are known, equations (B16) to (B23) of appendix B may be used to calculate corresponding values of after-mix kinetic energy loss coefficients. The trailing-edge loss in terms of kinetic energy may then be obtained from the difference between the two coefficients.

Calculation of Trailing-Edge Loss By the Method of Reference 6

The trailing-edge loss was obtained by using equation (10) of reference 6 (chap. 5, p. 6)

$$C_D = c_D \; 0.75 \; \sqrt[3]{\frac{t}{\delta_{full,\,tot}}} \tag{C17}$$

where c_D represents an independent drag coefficient determined by the geometry of the protuberance or trailing edge. A value of $c_D = 0.16$ was used which corresponded to the rounded trailing edge of the blading considered and $\delta_{full,\,tot}$ was calculated from the relation

$$\delta_{full,\,tot} = \delta_{tot}\left(\frac{1}{n} + 1\right) \tag{C18}$$

where values of δ_{tot} and n were obtained from previously described analytical calculations.

The trailing-edge drag coefficient was used to obtain an equivalent momentum thickness for the trailing-edge loss from the relation

$$\theta_{te} = \frac{C_D t}{2} \tag{C19}$$

With known values of equivalent momentum thickness and the assumption that the frictional boundary-layer thickness factors apply to the trailing-edge loss, the corresponding losses in terms of kinetic loss coefficients were calculated from equations presented in this appendix and appendix B.

APPENDIX D

EFFECT OF BLADE-EXIT STATIC PRESSURES ON LOSS COEFFICIENTS

Effect of Probe Blockage on Blade-Exit Static Pressures and Loss Coefficients

To calculate values of blade-exit boundary-layer loss characteristics, the flow conditions corresponding to the loss must be known. As noted under TEST PROCEDURE, the probe was found to obstruct the flow since, under steady-state conditions at the inlet and downstream stations, the presence of the probe in the channel affected the wall-tap blade-exit static pressures of that channel. Separate measurements of these wall-tap pressures were therefore made during testing. The pressures at blade exit when boundary-layer thickness was being measured in the same channel are the blade-exit pressures at which loss occurred and were used to establish free-stream conditions at the inner and outer radii at station 2 (see fig. 4, p. 6). In addition, to determine the effect on loss quantities of differences in blade-exit static pressure resulting from probe blockage, values of wall-tap static pressures at station 2 obtained from circumferential locations that were unaffected by the probe were also used to established free-stream conditions at the inner and outer radii.

An example of differences in blade-exit static pressures caused by flow obstruction due to probe blockage at design hub-section critical velocity ratio is shown in figure 14. The wall-tap blade-exit static pressures shown in figure 14 for obstructed flow were measured while loss was being measured in the same channel with the total-pressure probe. The effect of these differences on annular-sector after-mix loss coefficients over the range of critical velocity ratios investigated is shown in figure 15. (Values of loss coefficients shown are based on radial integration of circumferential loss characteristics, linear radial distribution of blade-exit static pressures, and the assumption that flow conditions at the blade mean section are representative of average flow conditions in the annular sector.) Figure 14 shows that blade-exit static pressures at design critical velocity ratio were significantly affected by probe obstruction. Figure 15 shows, at near design and lower critical velocity ratios, the loss coefficients based on obstructed flow to be a little larger than the loss coefficients based on unobstructed flow. The difference in loss coefficients varies from about 0.002 to 0.003.

From these results it was concluded that, for this range of critical velocity ratios, the loss coefficients had not been sufficiently affected by the difference in blade-exit static pressure due to probe blockage to be unreliable. The conclusion was based on the assumption that, for given free-stream conditions, the boundary-layer and trailing-edge losses would not be influenced by the presence of the probe. At critical velocity ratios

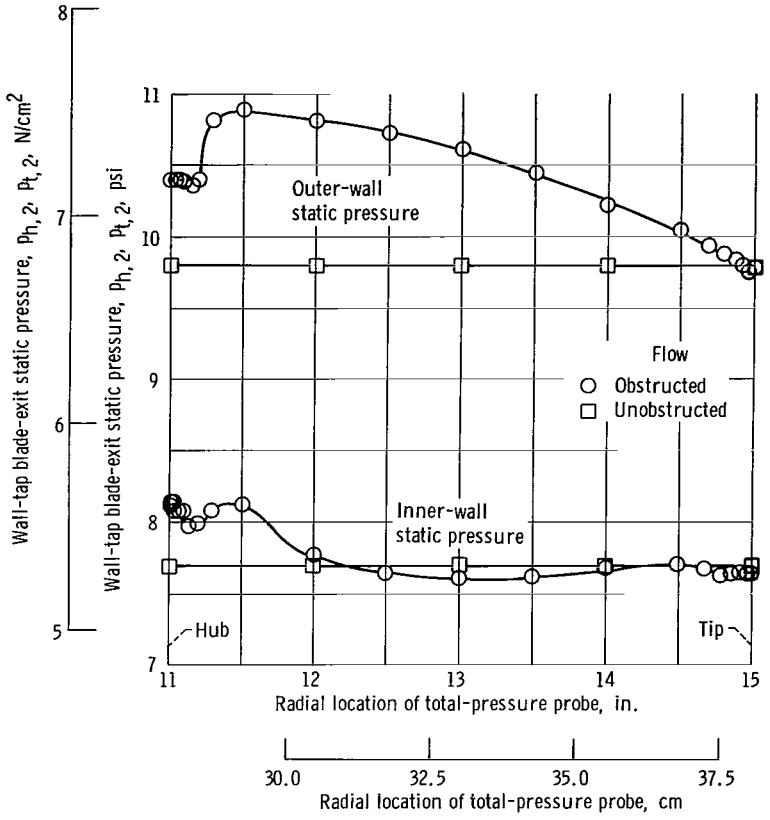

Figure 14. - Effect of probe blockage on wall-tap blade-exit static pressures at design hub-section critical velocity ratio.

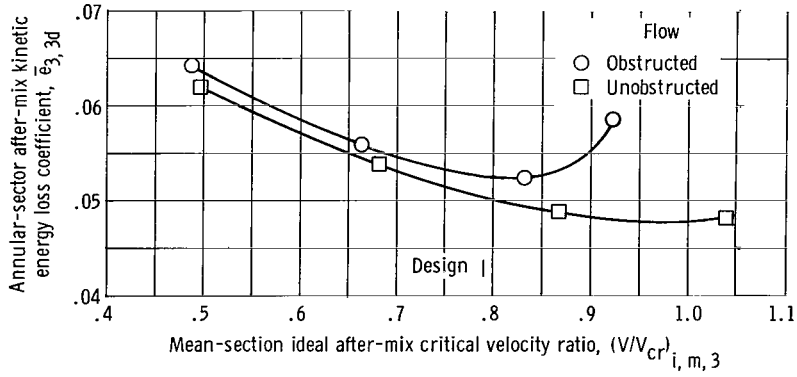

Figure 15. - Effect of probe blockage on annular-sector after-mix loss coefficients as function of critical velocity ratio.

above 0.832, differences in loss coefficients resulting from flow obstruction are so large that the results are considered unreliable and are therefore not considered herein. Since the blade losses were measured with the flow obstructed by the probe, the remaining loss values reported were based on free-stream conditions with obstructed flow.

Effect of Blade-Exit Radial Pressure Distribution On Loss Coefficients

After blade-exit static pressures are established at the inner and outer radii as described in the preceding section, the radial variation in pressure must be determined in order to obtain values of experimental loss characteristics at given radii. Two methods were used. A linear variation with radius was considered to obtain results consistent with the results reported for the reference blading. In addition, a linear divergence from free-vortex radial pressure distribution was used to determine its effect on loss quantities. It is believed that, even with flow distortion due to probe blockage, this distribution better represents the actual radial variation in blade-exit static pressure for a stator with free-vortex design.

Figure 16 shows, at an after-mix critical velocity near design, the variation in blade-exit pressures with radius that results from the two radial pressure distributions considered, and figure 17 shows the effect of these radial-pressure distributions on annular-sector, after-mix loss coefficients over the range of critical velocities considered. (Values of loss coefficients shown were obtained from radial integrations and

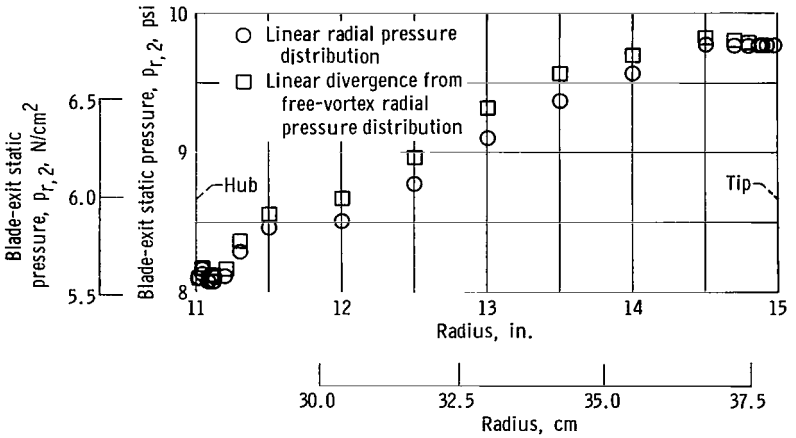

Figure 16. - Variation in blade-exit static pressure with radius for different assumptions of radial pressure distribution of design hub-section critical velocity ratio.

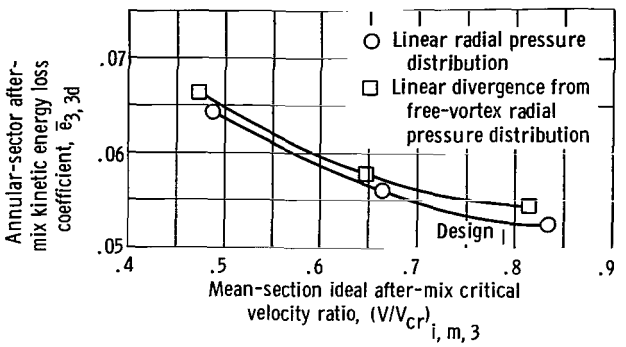

Figure 17. - Effect on annular-sector after-mix loss coefficients of different radial pressure distributions as function of after-mix critical velocity ratio.

assume that mean-radius, free-stream flow conditions are representative of the average free-stream flow conditions in the annular sector.) The loss coefficients based on linear divergence from free-vortex radial pressure distribution (fig. 17) are a little larger, about 0.001 to 0.002, than the loss coefficients based on linear radial pressure distribution. Since the differences are relatively small, to be consistent with the results reported for the reference blading, the results presented herein were based on linear radial pressure distribution.

REFERENCES

1. Dugan, J. F., Jr.; Koenig, R. W.; Whitlow, J. B., Jr.; and McAuliffe, T. B.: Power for the Mach 3 SST. Astronautics and Aeronautics, vol. 2, no. 9, Sept. 1964, pp. 44-51.

2. Whitney, Warren J.; Szanca, Edward M.; Moffitt, Thomas P.; and Monroe, Daniel E.: Cold-Air Investigation of a Turbine For High-Temperature-Engine Application. I. Turbine Design and Overall Stator Performance. NASA TN D-3751, 1967.

3. Stewart, Warner L.: Analysis of Two-Dimensional Compressible-Flow Loss Characteristics Downstream of Turbomachine Blade Rows in Terms of Basic Boundary-Layer Characteristics. NACA TN 3515, 1955.

4. Stewart, Warner L.; Whitney, Warren J.; and Wong, Robert Y.: Use of Mean-Section Boundary-Layer Parameters in Predicting Three-Dimensional Turbine Stator Losses. NACA RM E55L12a, 1956.

5. Whitney, Warren J.; Stewart, Warner L.; and Miser, James W.: Experimental Investigation of Turbine Stator-Blade-Outlet Boundary-Layer Characteristics and a Comparison with Theoretical Results. NACA RM E55K24, 1956.

6. Hoerner, Sighard F.: Fluid-Dynamic Drag. Midland Park, N.J., 1965.

7. Miser, James W.; Stewart, Warner L.; Wong, Robert Y.: Effect of a Reduction in Stator Solidity on Performance of a Transonic Turbine. NACA RM E55L09a, 1956.

NASA-Langley, 1968 —— 12 E-4165

"The aeronautical and space activities of the United States shall be conducted so as to contribute . . . to the expansion of human knowledge of phenomena in the atmosphere and space. The Administration shall provide for the widest practicable and appropriate dissemination of information concerning its activities and the results thereof."

—NATIONAL AERONAUTICS AND SPACE ACT OF 1958

NASA SCIENTIFIC AND TECHNICAL PUBLICATIONS

TECHNICAL REPORTS: Scientific and technical information considered important, complete, and a lasting contribution to existing knowledge.

TECHNICAL NOTES: Information less broad in scope but nevertheless of importance as a contribution to existing knowledge.

TECHNICAL MEMORANDUMS: Information receiving limited distribution because of preliminary data, security classification, or other reasons.

CONTRACTOR REPORTS: Scientific and technical information generated under a NASA contract or grant and considered an important contribution to existing knowledge.

TECHNICAL TRANSLATIONS: Information published in a foreign language considered to merit NASA distribution in English.

SPECIAL PUBLICATIONS: Information derived from or of value to NASA activities. Publications include conference proceedings, monographs, data compilations, handbooks, sourcebooks, and special bibliographies.

TECHNOLOGY UTILIZATION PUBLICATIONS: Information on technology used by NASA that may be of particular interest in commercial and other non-aerospace applications. Publications include Tech Briefs, Technology Utilization Reports and Notes, and Technology Surveys.

Details on the availability of these publications may be obtained from:

SCIENTIFIC AND TECHNICAL INFORMATION DIVISION

NATIONAL AERONAUTICS AND SPACE ADMINISTRATION

Washington, D.C. 20546